(#118)

An Investigation of Low Earth Orbit Internal Charging

L. Neergaard Parker, J. I. Minow, E. M. Willis

***Abstract*— Internal charging is not generally considered a threat in low Earth orbit due to the relatively short exposure times and low flux of electrons with energies of a few MeV encountered in typical orbits. There are configurations, however, where insulators and ungrounded conductors used on the outside of a spacecraft hull may charge when exposed to much lower energy electrons of some 100's keV in a process that is better characterized as internal charging than surface charging. We investigate the conditions required for this internal charging process to occur in low Earth orbit using a one-dimensional charging model and evaluate the environments for which the process may be a threat to spacecraft.**

Keywords—charging; low Earth orbit

I. INTRODUCTION

Low Earth orbit (LEO) is usually considered a relatively benign environment for internal charging threats due to the low flux of penetrating electrons with energies of a few MeV that are encountered over an orbit. There are configurations, however, where insulators and ungrounded conductors used on the outside of a spacecraft hull may charge when exposed to much lower energy electrons of some 100's keV in a process that is better characterized as internal charging than surface charging. For example, the minimal radiation shielding afforded by thin thermal control materials such as metalized polymer sheets (e.g., aluminized Kapton® or Mylar) and multilayer insulation (MLI) may allow electrons of 100's of keV to charge underlying materials. Yet these same thermal control materials protect the underlying insulators and ungrounded conductors from surface charging currents due to electrons and ions at energies less than a few keV as well as suppress the photoemission, secondary electron, and backscattered electron processes associated with surface charging.

The Internal Charging Model (I.cam) was developed by Marshall Space Flight Center's Natural Environments Branch to help flight projects understand the radiation shielding requirements in different spacecraft orbits required to mitigate charging for different material configurations. The user can specify specific material configurations and the energy range of penetrating energetic electrons that charge materials under thin shielding. The model then calculates the internal electric field due to accumulating charge and compares result to the breakdown strength of the material in order to determine if there is a threat for arcing.

This paper describes an investigation using the I.cam model into the conditions required for this low Earth orbit "internal charging" process to occur and provides examples of the environments for which the process represents a threat to spacecraft. First, we describe the simple one-dimensional I.cam internal charging model that is used to compute the charge accumulation on materials under thin shielding. Only the electron flux that penetrates exposed surface shielding material is considered and we treat the charge balance in underlying insulation as a parallel plate capacitor accumulating charge from the penetrating electron flux and losing charge due to conduction to a ground plane. Charge dissipation due to conduction can be neglected to consider the effects of charging an ungrounded conductor. In both cases, the potential and electric field is computed as a function of time. An additional charge loss process is introduced due to an electrostatic discharge current when the electric field reaches prescribed breakdown strength. For simplicity, the amount of charge lost in the discharge is treated as a random percentage of the total charge between a set maximum and minimum amount so a user can consider partial discharges of insulating materials (small loss of charge) or arcing from a conductor (large loss of charge). We then apply the model using electron flux measurements from a National Oceanic and Atmospheric Administration (NOAA) spacecraft in LEO to demonstrate that charging can reach levels where electrostatic discharges occur and estimate the magnitude of the discharge.

II. MODEL DEVELOPMENT

The model numerically solves equation (1) for the internal electric field, where ϵ is permitivity, **E** is the electric field, σ is the conductivity of the material, and **J** is current density [1] for each point along the orbit.

$$\epsilon \frac{d\bar{E}}{dt} + \sigma \bar{E} = \bar{j} \tag{1}$$

Potential (φ) and stored charged (Q) are computed for each timestep as well. The model has the capability to enable enhancement of the electric field due to sharp corners. If no enhancement is desired, the value is set to 1. The capacitance of the material configuration is calculated assuming a parallel plate capacitor model. The capacitance model can be modified in future versions to consider spherical and/or cylindrical capacitor models as well. Once the electric field has been calculated, it is compared to the electric breakdown

L. Neergaard Parker is with Jacobs ESSSA Group, Huntsville, AL, 35806 USA (e-mail: Linda.Parker@nasa.gov)

J. I. Minow and E. M. Willis are with NASA/MSFC, Huntsville, AL, 35816

strength (E_{bd}) of the material, which is a user provded value. If $\mathbf{E} < \mathbf{E}_{bd}$, then the model goes to the next timestep and recalculates E, φ, and Q based on the new input current density J which continues until the electric field meets or exceeds the electric breakdown strength.

When the electric field condition $\mathbf{E} \geq \mathbf{E}_{bd}$ is met the model simulates charge loss through an electrostatic discharge arc. Arcs are simulated by assigning a random amount of charge loss as a percentage of the total accumulated charge density within a set discharge percentage range. The discharge percentage range is a user input between 0 (minimum possible) and 1 (maximum possible). We typically assume maximum and minimum discharge values near 1 for conductors where the entire charge density can couple to the arc and values in the 0.1 to 0.3 range for insulators where only a fraction of the total charge is typically lost in an arc. Post arc values of the electric field, potential, and charge on the material are calculated and compared to the pre-arc values to yield information about the strength of the discharge produced, such as energy in the arc and current pulses for three arc discharge time constants. These quantities are stored in an output file for future use and analysis.

The input electron current density J along a satellite trajectory is obtained from satellite measurements of electron flux in LEO orbits. For the results shown here we have used electron data from the Medium Energy Proton and Electron Detector (MEPED) instrument on the NOAA-19 Polar-orbiting Operational Environmental Satellite (POES) satellite for a period from October 2011 to the end of December 2012. The NOAA-19 POES spacecraft is a three axis-stabilized platform in a sun-synchronous orbit at an altitude of 870 km and 98.7° inclination. The MEPED solid state detector [2] includes three integral electron channels covering the energy ranges 30-1100 keV, 100-1100 keV, and 300-1100 keV. There are two electron telescopes with 0° (zenith) and 90° (horizontal) look angles. The 0° detector observes the geomagnetically trapped electrons at low latitudes and those particles caught in the atmospheric loss cone at higher latitudes. Conversely, the 90° detector monitors those particles in the loss cone at low latitudes and the geomagnetically trapped particles at higher latitudes. Each detector has a 15° half angle field of view. We have used the 16 second average electron flux data available from NOAA for our work to date. It should be noted that the MEPED instrument can provide data in two second time resolution, but at this stage of model developemnt the finer time resolution is not required.

For the results in this work we have added the flux measurements (in units of electrons/cm^2-sec-sr) from both the zenith and horizontal detectors and multiply by π steradians assuming an isotropic flux distribution before converting to the current density required for input to the charging model. This algorithm possibly over estimates the environment, especially in the mid-latitude regions during geomagnetic quiet periods, but is a necessary assumption in the current stage of model development. We have explored options for fitting the data to pitch angle distributions but this work will not be shown here.

For each example case, we need to know the energy range that can penetrate a given shielding level and then deposit charge within a given depth of unground conductor or insulating material. We calculate the areal density of the shielding and charging target materials and use the range-energy relations provided by the National Institute of Standards and Technology (NIST) Electron Stopping-Power and Range Tables for Electrons (ESTAR) model to calculate the stopping range within the ungrounded or conducting material [3]. The charging model assumes electrons with minimum energy E_{min} required to penetrate the shielding material arrives at the front surface of the charging target material, electrons with maximum energy E_{max} penetrate to the back surface of the charging target material, and the charge that accumulates within the charging target material capacitance is given by the difference between the integral flux represented by $J(>E_{min})$ and $J(>E_{max})$.

An example for obtaining the minimum and maximum electron energies to be used in a charging case is shown in Fig. 1. Radiation shielding is provided by a 10-layer MLI stack consisting of individual 1-mil thick Kapton® layers and the charging target is a 5 mm thick sample of insulating Kapton® material. A mass density of 1.42 g/cm^3 is used for Kapton®. For the parameters stated, the fraction of the energy spectrum that will deposit charge in the insulating target material is approximately 150 keV – 900 keV. We can assume that the MLI shielding has suppressed any moderation of charging afforded by the secondary electron which is an important process in surface charging because the minimum energy required to penetrate the shielding is 150 keV, an energy where secondary electron yields are negligible for most materials and any low energy secondary electrons emitted with energies of a few eV will not be able to penetrate the MLI stack [4,5].

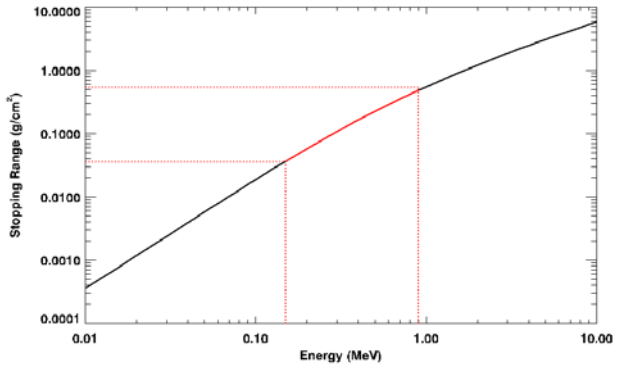

Fig. 1. Stopping range calculated for 10 layers of MLI at 1 mil each.

The model interpolates the integral electron current density at the minimum and maximum energies from the MEPED electron spectrum and then takes the difference to obtain the

total current density deposited in the charging target during a time step.

III. EXAMPLES

We present here three examples of charging an insulating target material by eneretic electrons from the space environment with charge loss through conduction to ground and arcing. The three examples have different input parameters selected to illustrate the impact that differences in satellite material configuration can have on charging and electrostatic discharge levels in LEO. Table 1 lists parameters used in the model run for Example 1. These values are the same for the subsequent examples except where specifically defined within the text for Examples 2 and 3.

Table 1. Model input parameters.

Parameter	Value
Mimimum threshold energy (keV)	150
Maximum threshold energy (keV)	900
Dielectric constant	4.0
Thickness of ungrounded material (mm)	5.0
Length of ungrounded material (cm)	100
Width of ungrounded material (cm)	100
Volume resistivity (Ω·m)	10^{18}
Material breakdown strength (V/m)	$2.5x10^{7}$
E-field enhancement	1.0
Maximum arc discharge	0.3
Minimum arc discharge	0.1
Discharge time A (μ sec)	0.1
Discharge time B (μ sec)	1
Discharge time C (μ sec)	10

A. *Example 1*

The first example studied simulates a 100 cm x 100 cm sheet of insulating Kapton® material under 10 mils of MLI shielding. The depth of the Kapton® charging target material is 5 mm. Fig 2. illustrates this geometry. NIST ESTAR was used to calculate the penetration depth of electrons. For this example (using the same parameters from the previous seciton) we find electrons in the energy of 150-900 keV are able to penetrate the MLI shielding and deposit charge in the charging target material underneath the MLI shielding.

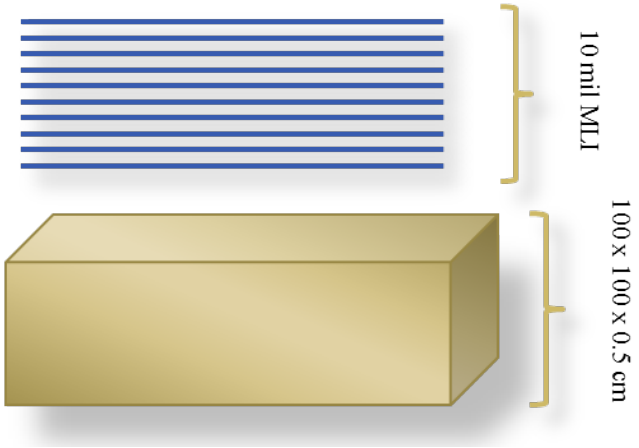

Fig. 2. Material geometry used in Example 1.

This configuration produced four discharges. These are shown at the corresponding discharge time in Fig. 3 as the vertical orange lines and at the corresponding point along the orbit in Fig. 4 as the red points. The energy discharged was between 10-30% of the total energy stored in the capacitance, producing arc energies in the ten's of Joules. Specific information about each discharge is stored in an output file, shown in Table 2. Each simulated discharge will have information for when the arc occurred, what fraction of the stored charge density was discharged in the arc, voltage difference across the target material thickness. Also computed are the arc currents assuming three different scales for discharge times and the energy in the resulting arcs.

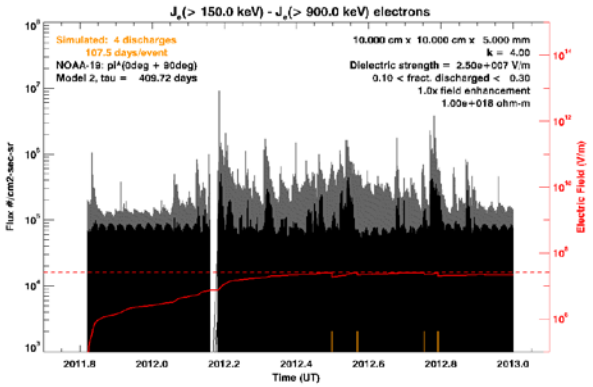

Fig. 3 Simulated arcs for Example 1. Plotted is flux as a function of time, as well as electric field (right vertical axis in red) as a function of time.

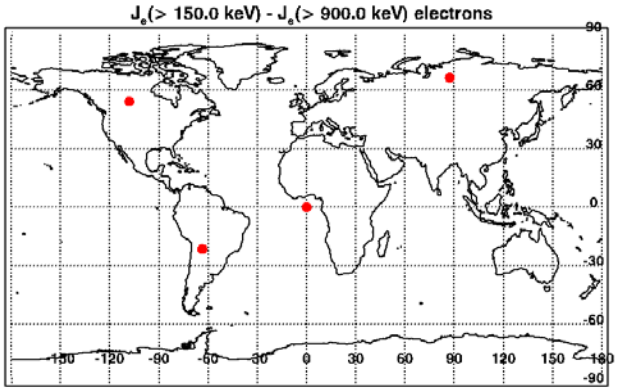

Fig 4. Locations of electrostatic discharges along the orbit for Example 1.

The model also generates a map shown in Fig. 4. of discharge locations based on the NOAA-19 satellite ephemeris and time along the orbit where the discharges occur. This feature is useful for comparing the distributions of arc locations against spacecraft anomaly events in anomaly investigations.

Table 2. Output parameters for each discharge in Example 1.

Time of discharge (UT)	Fraction discharged	φ before arc (volts)	φ after arc (volts)	Arc energy (mJ)	Arc current (0.1 μ sec)	Arc current (1.0 μ sec)	Arc current (10.0 μ sec)
2012.4995	0.1515	125000.1	106058.5	15493.1982	1340	134	13.4
2012.5434	0.1894	125003	101324.3	18971.375	1680	168	16.8
2012.655	0.2437	125000.2	94539.2	23673.375	2160	216	21.6
2012.7985	0.2055	125000.5	99307.8	20401.3105	1820	182	18.2

B. *Example 2*

We next modify the configuration used in the first example as shown in Fig. 5. to simulate a case with 5 mils of MLI shielding covering a charging target of 5 mm thick Kapton®, a configuration with 50% reduction in shielding compared to Example 1 but all other inputs the same. The reduced shielding results in a lower range of energies penetrating the MLI shielding (now 89-900 keV) but at a higher flux that will deposit a greater amount of charge in the underlying target material.

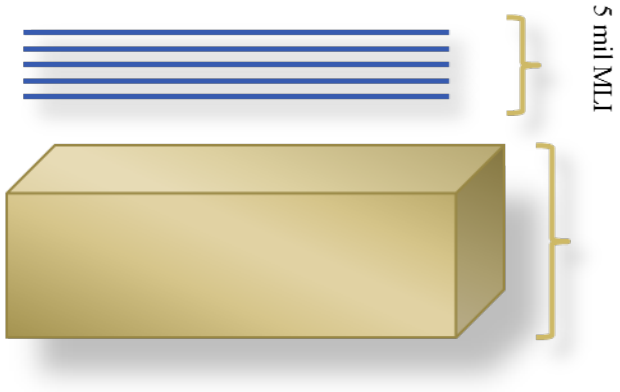

Fig. 5. Material geometry for Example 2.

This simple change of reducing the shielding by 50% results in an increase in the number of arcs to 16 discharges for the same external NOAA-19 electron environment used in the first example. The energy released for these arcs are now in the hundreds of Joule range while the arc currents calculated remain in the same order of magnitude.

C. *Example 3*

The final example to be discussed here uses 5 mils of MLI shielding. However, the ungrounded material is now 10 layers of MLI, each layer electrically connected to each other but electrically isolated from the spacecraft to simulate the effect of charging ungrounded layers of MLI. The material configuration is shown in Fig. 6. The total thickness of ungrounded material is reduced from Examples 1 and 2, resulting in a larger overall capacitance and the energy of electrons depositing charge in the target material ranges from 80-175 keV.

The code produced ten arcs for this configuration. The arc energies calculated are smaller than those produced in Examples 1 and 2. However, the number of discharges is more than twice as many as for Example 1 – indicating that while the amount of charge dissipated and the energy in each arc may be less than the first example, there are more arcs capable of damaging the material.

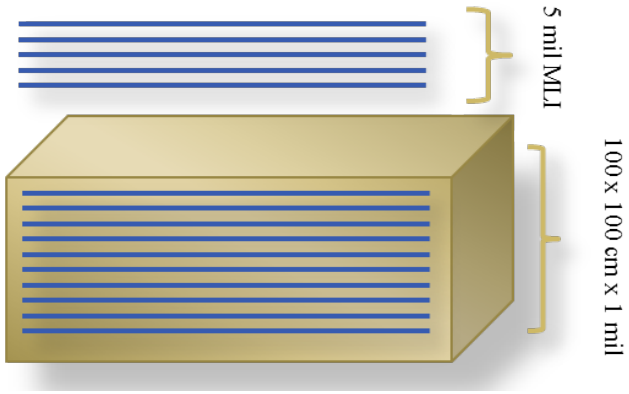

Fig. 6. Material geometry for Example 3.

IV. Summary

This paper describes an internal charging model developed in the Natural Environments Branch at Marshall Space Flight Center to help programs understand the shielding requirements of the different spacecraft configurations and orbits being considered. The model considers a layer of shielding over an insulating or ungrounded charging target material. Input parameters include the energy range for electrons that deposit charge in the charging target material, which is calculated externally, material properties such as dielectric constant, volume resistivity, breakdown strength, dimensions of the materials in question, the minimum and maximum discharge amounts which range between 0 and 1, respectively, and different discharge times. We find that as shielding decreases, the charge accumulation and associated electric fields of the charging target increases resulting in an increase in the number of discharges along an orbit. The ungrounded MLI produced a significant number of discharges even though the ungrounded layers were relatively thin.

The model also produces plots to show where the discharges occurred along the orbit, frequency of discharge, flux levels of the environment, and electric field strength. Additionally, an output file is produced with specific current and energy details for each arc. The output files can be used later to compare multiple runs or to produce additional plots. This information can be used to help programs understand the implications of the shielding design being proposed, as well as aid in anomaly investigations should that occur. Additional capabilities are being discussed for future model versions such as including the density of the material, the radiation induced conductivity, different capacitance models such as spherical and cylindrical, and additional orbit capabilities.

Acknowledgment

NOAA-19 electron data was provided courtesy of NOAA's National Geophysical Data Center.

References

[1] Garrett, H. and A. Whittlesey, "Spacecraft Charging, An Update," IEEE Transactions on Plasma Science,k Vol. 28, No. 6, December, 2000.

[2] Evans, D.S., and M.S. Greer, Polar Orbiting Environmental Satellite Space Environment Monitor – 2, Instrument Descriptions and Archive Data Documentation, SEM2v2, NOAA, 2006. URL:http://satdat.ngdc.noaa.gov/sem/poes/docs/sem2_docs/2006/SEM2v2.0.pdf

[3] URL: http://physics.nist.gov/PhysRefData/Star/Text/ESTAR.html.

[4] Whipple, E.C., Potentials of surfaces in space, Rep. Prog. Phys., 44, 1197 -1250, 1981.

[5] Katz, I., M. Mandell, G. Jongeward, and M.S. Gussenhoven, The importance of accurate secondary electron yields in modeling spacecraft charging, J. Geophys. Res., 91, 13739-13744, 1986.